10 Polarization Issues

The study of spin dynamics in synchrotrons has evolved over the years as has the desire for achieving polarized particle beams of the highest possible beam energies. A selection of reviews of the dynamics of polarized beams may be found in [1]–[9]. In this chapter, we focus on experimental data and describe spin transport in circular accelerators and transport lines. Except where explicitly mentioned, radiative effects in electron accelerators or very high energy proton accelerators are not treated here. We begin with a review of the Thomas-BMT equation for spin motion. This will be given in terms of the SU(2) spinor representation. Spinor algebra will be introduced and applied in the description of techniques used for preserving the beam polarization during acceleration through depolarizing resonances at moderate beam energies.

10.1 Equation of Spin Motion

The concept of particle spin was first introduced by Uhlenbeck and Goudsmit in 1926 to explain certain features of atomic spectra. They presupposed that the (in this case) electron of mass m and charge e, possessed both a magnetic moment $\boldsymbol{\mu}$ and the spin angular momentum $\boldsymbol{s}$, related to one another by

$$\boldsymbol{\mu} = \frac{ge}{2m}\boldsymbol{s} \,, \tag{10.1}$$

where g is the gyromagnetic ratio whose value was empirically taken to be 2 for electrons to explain certain experimental observations. In 1927 Thomas [10] showed that once a relativistic kinematic effect was taken into account, the value of $g = 2$ was consistent with the atomic spectra measurements.

The equation of motion for the spin angular momentum in an external magnetic field [5] is given, in the particle rest frame, by

$$\begin{aligned} \frac{\mathrm{d}\boldsymbol{s}}{\mathrm{d}t} &= \boldsymbol{\mu} \times \boldsymbol{B} \\ &= \boldsymbol{\Omega} \times \boldsymbol{s} \,, \end{aligned} \tag{10.2}$$

M. G. Minty et al., *Measurement and Control of Charged Particle Beams,*
https://doi.org/10.1007/978-3-662-08581-3_10

where the angular velocity of the spin precession is

$$\boldsymbol{\Omega} = -\frac{ge}{2m}\boldsymbol{B}. \tag{10.3}$$

In the above equations, the spin angular momentum $\boldsymbol{s}$ of a single particle takes on discrete values of magnitude $|\boldsymbol{s}| = \hbar/2$ for spin-$\frac{1}{2}$ particles (i.e. electrons and protons). It is convenient to normalize $\boldsymbol{s}$ and work with the spin vector $\boldsymbol{S}$, with $|\boldsymbol{S}| = 1$, defined as the normalized spin expectation value in the rest frame.

10.2 Thomas-BMT Equation

In the laboratory frame, the spin precession for a relativistic particle in external electromagnetic fields is given by the Thomas-BMT equation [10]–[13]:

$$\frac{\mathrm{d}\boldsymbol{S}}{\mathrm{d}t} = -\frac{e}{\gamma m}\left[(1+a\gamma)\ \boldsymbol{B}_\perp + (1+a)\ \boldsymbol{B}_\parallel + \left(a\gamma + \frac{\gamma}{\gamma+1}\right)\frac{\boldsymbol{E}\times\boldsymbol{v}}{c^2}\right]\times\boldsymbol{S}\ , \tag{10.4}$$

where $\boldsymbol{B}_\perp$ and $\boldsymbol{B}_\parallel$ represent the magnetic fields perpendicular and parallel to the particle velocity respectively, $\boldsymbol{\beta} = \boldsymbol{v}/c$ with $\boldsymbol{v}$ the particle velocity, and $\gamma = 1/\sqrt{1-\beta^2}$ the Lorentz factor or ratio of the particle energy to mass.

The factor a in (10.4) is the gyromagnetic anomaly of the electron. It is

$$a = \frac{g-2}{2} = 0.00115966\ , \tag{10.5}$$

and deviates from zero due to radiative corrections. For protons, which are composite, we replace a with the symbol G, where

$$G = \frac{g-2}{2} = 1.792846\ . \tag{10.6}$$

For many practical applications there are no significant electric fields[1], and the Thomas-BMT equation is simply

$$\frac{\mathrm{d}\boldsymbol{S}}{\mathrm{d}t} = -\frac{e}{\gamma m}\left[(1+a\gamma)\boldsymbol{B}_\perp + (1+a)\boldsymbol{B}_\parallel\right]\times\boldsymbol{S}\ . \tag{10.7}$$

From this equation applied to protons, the spin precession due to transverse magnetic fields depends on the particle energy through the factor $1/\gamma + G$ while the amount of precession due to a longitudinal magnetic field scales as $(1+G)/\gamma$. We will see later that this has implications for spin rotator design.

[1] More precisely, the term $\boldsymbol{\beta}\times\boldsymbol{E}$ is nearly zero since the electric fields in an accelerator are usually parallel to the particle velocity.

10.3 Beam Polarization

The polarization $\mathbf{P}$ of a bunch is defined as the ensemble average over the spin vectors $\boldsymbol{S}$ of the individual particles:

$$\mathbf{P} = \langle \boldsymbol{S} \rangle = \left| \frac{1}{N} \sum_{p=1}^{N} \boldsymbol{S}_p \right| , \tag{10.8}$$

where N denotes the number of particles in the bunch.

As an illustration of the formulae presented so far, we calculate the beam depolarization due to spin precession and energy spread in a transport line neglecting radiation effects. We suppose a transverse magnetic field bends an electron orbit by the angle θ. Then, according to (10.4) one finds that the electron spin direction precesses by $\phi = (a\gamma)\theta$ relative to the orbit in the laboratory frame. Considering a relativistic electron beam of many particles with a finite energy spread, the spin vectors of different electrons in the beam precess by different angles, since ϕ depends on the particle energy. If the initial beam polarization is longitudinal with magnitude P_0 and the beam is bent horizontally by an angle θ, not only is the final polarization vector $\mathbf{P}_f$ rotated by an angle $a\gamma_0\theta$, but also its magnitude is reduced as

$$P_f = P_0 e^{-(a\gamma_0\sigma_\delta\theta)^2/2} , \tag{10.9}$$

where γ_0 is the Lorentz factor corresponding to the mean energy of the beam, and σ_δ the rms relative momentum spread assuming a Gaussian momentum distribution. Equation (10.9) is strictly valid, if the orbit is bent in one plane. The same formula was also used to model the spin transport and the depolarization in the SLC North Collider Arc [14, 15], which constituted a nonplanar transport line with horizontal and vertical bends used to follow the terrain of the SLAC site. In this application, an 'effective' bending angle θ, entering in (10.9), was determined by measuring the final direction of the polarization vector as a function of the beam energy [15].

10.4 Spinor Algebra Using SU(2)

We can use methods of quantum mechanics [5] to describe spin transport. It is mathematically advantageous to do so since transporting 2 component spinors (Ψ) is simpler than transporting the 3-dimensional spin vector $\boldsymbol{S}$. The relationship between the two is given by

$$S_i = \Psi^\dagger \sigma_i \Psi , \tag{10.10}$$

with the Pauli matrices defined[2] as

[2] Caution. Different authors adopt different conventions; here we adopt the convention (specified in the introduction; c.f. Fig. 1.1) that x is radial, s is longitudinal, and y is vertical. A cyclic permutation may be used to transform between conventions.

$$\sigma_x = \begin{pmatrix} 0 & 1 \\ 1 & 0 \end{pmatrix} , \quad \sigma_s = \begin{pmatrix} 0 & -\mathrm{i} \\ \mathrm{i} & 0 \end{pmatrix} , \quad \sigma_y = \begin{pmatrix} 1 & 0 \\ 0 & -1 \end{pmatrix} . \tag{10.11}$$

Together with the 2×2 identity matrix I_2, these 4 matrices generate an irreducible representation of the SU(2) group.

10.5 Equation of Spin Motion

For generality we can reexpress [1] the equation of spin motion (10.2) in terms of a time-like variable θ defined as

$$\theta = \int_0^s \frac{\mathrm{d}s'}{\rho(s')} , \tag{10.12}$$

which is equal to the accumulated bending angle or so-called orbital angle. Then, as we will show below, the equation of spin motion (10.2) is equivalent to

$$\frac{\mathrm{d}\Psi}{\mathrm{d}\theta} = \frac{i}{2} H \Psi , \tag{10.13}$$

where $H = \tilde{\boldsymbol{\Omega}} \cdot \boldsymbol{\sigma}$ denotes the effective spin Hamiltonian, which is represented here as a matrix [5] with

$$\tilde{\boldsymbol{\Omega}} = \boldsymbol{\Omega} / \frac{\mathrm{d}\theta}{\mathrm{d}t} . \tag{10.14}$$

In the absence of depolarizing resonances (see Sect. 10.7), for a particle circulating in the horizontal plane under the influence of vertical magnetic fields only, H may be expressed as

$$H = \begin{pmatrix} -\kappa & 0 \\ 0 & \kappa \end{pmatrix} , \tag{10.15}$$

with $\kappa = G\gamma$ for protons and $\kappa = a\gamma$ for electrons.

Equation (10.13) may be expressed as

$$\frac{\mathrm{d}\Psi}{\mathrm{d}\theta} = -\mathrm{i} \frac{\lambda}{2} (\boldsymbol{\sigma} \cdot \hat{\boldsymbol{b}}) \Psi , \tag{10.16}$$

where $\lambda = |\tilde{\boldsymbol{\Omega}}|$ denotes the amplitude of the precession frequency and depends in general on the particle coordinates (to concentrate on the underlying principles, we defer the explicit expressions until needed in Sect. 10.12) and $\hat{\boldsymbol{b}} = \hat{\boldsymbol{\Omega}}$ is a unit vector aligned with the precession axis. The vector $\hat{\boldsymbol{b}}$ and λ depend on the longitudinal coordinate and on the position of the particle in the six-dimensional phase space [7]. Therefore $\hat{\boldsymbol{b}}$ may have different orientations at fixed orbital angle θ on subsequent turns.

The solution of (10.16), which defines the spinor transformation matrix M, is

$$\Psi(\theta) = M \Psi(0) . \tag{10.17}$$

If $\lambda\hat{b}$ is constant along a section of the orbit, then

$$M = e^{-\mathrm{i}(\frac{\lambda}{2})(\boldsymbol{\sigma}\cdot\hat{\boldsymbol{b}})\theta} \,. \tag{10.18}$$

Using the algebra of the σ matrices, after expanding the exponential, the solution for the spinor is

$$\Psi(\theta) = \left[\cos\left(\frac{\lambda\theta}{2}\right) - i(\boldsymbol{\sigma}\cdot\hat{\boldsymbol{b}})\sin\left(\frac{\lambda\theta}{2}\right)\right]\Psi(0) \,. \tag{10.19}$$

To complete this section we use the Pauli algebra to confirm that the equation of motion for the spinor Ψ (10.13) indeed leads to the equation of motion for the spin vector $\mathbf{S}$. Since the components of the spin are given by the expectation value of the Pauli spin matrices ($\mathbf{S} = \Psi^\dagger\boldsymbol{\sigma}\Psi$), the equation of spin motion for the polarization vector is obtained by taking the derivative of the latter expression

$$\frac{\mathrm{d}\mathbf{S}}{\mathrm{d}\theta} = \frac{\mathrm{d}\Psi^\dagger}{\mathrm{d}\theta}\boldsymbol{\sigma}\Psi + \Psi^\dagger\boldsymbol{\sigma}\frac{d\Psi}{d\theta} \,. \tag{10.20}$$

Using (10.16) and its Hermitian conjugate, $\frac{\mathrm{d}\Psi^\dagger}{\mathrm{d}\theta} = \mathrm{i}\frac{\lambda}{2}\Psi^\dagger(\boldsymbol{\sigma}\cdot\hat{\boldsymbol{b}})$, one finds

$$\frac{\mathrm{d}\mathbf{S}}{\mathrm{d}\theta} = i\frac{\lambda}{2}\Psi^\dagger[(\boldsymbol{\sigma}\cdot\hat{\boldsymbol{b}})\boldsymbol{\sigma} - \boldsymbol{\sigma}(\boldsymbol{\sigma}\cdot\hat{\boldsymbol{b}}))]\Psi \,. \tag{10.21}$$

Making use of the Pauli algebra $\sigma_i\sigma_j = 1$ for $i = j$ and $\sigma_i\sigma_j = i\epsilon_{ijk}\sigma_k$ for $i \neq j$, one can show that

$$[\boldsymbol{\sigma}\cdot\hat{\boldsymbol{b}}, \boldsymbol{\sigma}] = 2\mathrm{i}(\hat{\boldsymbol{b}}\times\boldsymbol{\sigma}) \,. \tag{10.22}$$

Therefore, we may write

$$\frac{\mathrm{d}\mathbf{S}}{\mathrm{d}\theta} = -\lambda\Psi^\dagger(\hat{\boldsymbol{b}}\times\boldsymbol{\sigma})\Psi = -\lambda\hat{\boldsymbol{b}}\times(\Psi^\dagger\boldsymbol{\sigma}\Psi) = -\lambda(\hat{\boldsymbol{b}}\times\mathbf{S}) \,, \tag{10.23}$$

which may be compared with (10.4).

10.6 Periodic Solution to the Equation of Spin Motion

The first step for studying spin motion in a circular accelerator is to find the periodic solution to the equation of spin motion on the closed orbit. Here we write a spin transfer matrix M as a product of n precession matrices, each of which characterizes a section of constant magnetic field causing spin precession; i.e., $M = M_1M_2\cdots M_n$.

The transfer matrix corresponding to one turn around the accelerator is refered to as the one turn spin transfer map denoted by M_0. For the closed orbit M_0 is periodic: $M_0(\theta + 2\pi) = M_0(\theta)$. Because the norm of the vector

in the precession equation is an invariant, M_0 is unitary so that it may be expressed as

$$M_0 = e^{-\mathrm{i}\pi\nu_0(\boldsymbol{\sigma}\cdot\hat{\boldsymbol{n}}_\mathbf{0})} = I_2 \cos\pi\nu_0 - i(\boldsymbol{\sigma}\cdot\hat{\boldsymbol{n}}_\mathbf{0})\sin\pi\nu_0 \ , \tag{10.24}$$

or

$$M_0 = \begin{pmatrix} \cos\pi\nu_0 - \mathrm{i}\sin\pi\nu_0\cos\alpha_y & -\sin\pi\nu_0\cos\alpha_s - \mathrm{i}\sin\pi\nu_0\cos\alpha_x \\ \sin\pi\nu_0\cos\alpha_s - \mathrm{i}\sin\pi\nu_0\cos\alpha_x & \cos\pi\nu_0 + \mathrm{i}\sin\pi\nu_0\cos\alpha_y \end{pmatrix} , \tag{10.25}$$

The unit vector $\hat{\boldsymbol{n}}_\mathbf{0}$ is the precession axis for the one turn map M_0. It is periodic and fulfills the Thomas-BMT equation [5]; a spin set parallel to $\hat{n}_0$ at orbital location θ will, after one turn $(\theta + 2\pi)$, also be parallel to $\hat{n}_0$. Thus $\hat{n}_0$ is refered to as the 'stable spin direction' on the closed orbit and may be described by direction cosines:

$$\hat{\boldsymbol{n}}_\mathbf{0} = (\cos\alpha_x, \cos\alpha_s, \cos\alpha_y) \tag{10.26}$$

with normalization $\cos^2\alpha_x + \cos^2\alpha_s + \cos^2\alpha_y = 1$.

The parameter ν_0, called the spin tune, represents the number of times the spin of a particle on the closed orbit precesses about the stable spin direction in one turn around the ring. The fractional part of the spin tune may be obtained from the trace of the (periodic) spin precession matrix:

$$\begin{aligned} \mathrm{Tr}\ M_0 &= 2\cos\pi\nu_0 \quad \text{or} \\ \nu_0 \quad &= \frac{1}{\pi}\cos^{-1}\left(\frac{\mathrm{Tr}\ M_0}{2}\right) . \end{aligned} \tag{10.27}$$

For the spin motion of particles not on the closed orbit, M is in practice not periodic since accelerators are not typically operated on resonance (for which the particle returns to the same point in phase space after an integer number of turns). The unit vector $\hat{\boldsymbol{b}}$ in the equation of spin motion (10.16) may therefore have different orientations at fixed orbital coordinate θ on subsequent turns $(\theta, \theta + 2\pi, \theta + 4\pi, ...)$.

10.7 Depolarizing Resonances

The spin of a particle executing synchro-betatron motion around the closed orbit is perturbed by magnetic fields sampled at the betatron and synchrotron frequencies which are characteristic of the particle motion. Since the particles within a bunch have generally different amplitudes and phases, the perturbation to the spin is different for different particles resulting in a spread of the particle spins and thus a lower polarization.

Depolarizing resonances occur whenever the spin tune beats with any of the natural oscillation frequencies of the orbital motion; that is when the spin tune, ν_0, equals a resonance tune, $\nu_{\rm res}$, by satisfying

$$\nu_0 = \nu_{\rm res} \equiv m + qQ_x + rQ_y + sQ_s \ , \tag{10.28}$$

where Q_x and Q_y are the horizontal and vertical betatron tunes, Q_s is the synchrotron tune, while m, q, r,and s are integers[3]. Here m is the product of an integer times the periodicity of the lattice. The quantity $|q| + |r| + |s|$ is called the order of the resonance.

The general resonance condition specifies the criteria for many different types of resonances. Imperfection depolarizing resonances, for which

$$\nu_0 = \nu_{\rm res} = m = \text{integer} \ , \tag{10.29}$$

arise, for example, from horizontal magnetic fields experienced by the orbiting particle due to magnet imperfections, dipole magnet rotations about the beam direction, and to vertical quadrupole magnet misalignments. Lowest order intrinsic resonances, which result from the horizontal fields of quadrupoles, occur if

$$\nu_0 = \nu_{\rm res} = m + rQ_y \ . \tag{10.30}$$

In practice, the above two types of resonances have proven the most significant in the energy regimes of existing accelerators with polarized beams.

Other higher order spin depolarizing resonances may occur for any combination of integers which satisfy (10.28). Studies have shown that higher-order intrinsic resonances of the form

$$\nu_0 = \nu_{\rm res} = m + rQ_y + sQ_s \ . \tag{10.31}$$

become increasingly important at higher beam energies. Due to the interaction with the particle longitudinal momentum, such resonances are also refered to as synchrotron sideband depolarizing resonances.

Resonant spin motion has been observed in many accelerators. Interestingly, it was observed in the SLC collider arcs [14], through which bunches pass only once. The 1 mile arcs were used to transport 45.6 GeV polarized electrons from the linac to the interaction point where they collided head-on with positrons. The arc consists of 23 achromatic sections with a 108° phase advance per cell. The vertical beam trajectory and the components of a spin vector are shown in Fig. 10.1 assuming an initial vertical offset of 0.5 mm and random quadrupole misalignments. For the nominal SLC operating energy, the phase advances of (betatron) orbit and spin in the SLC arcs were almost identical. In Fig. 10.1 this equality is seen to contribute to a net tilt of the spin vector as evidenced by the increase in the vertical component of a spin along the arc. In practice, vertical bumps were used to optimally align the polarization to be longitudinal at the interaction point.

[3] For particles in the bunch with large orbital amplitudes, ν_0 in (10.28) should be replaced by spin tune of the individual particle ν [7]–[9].

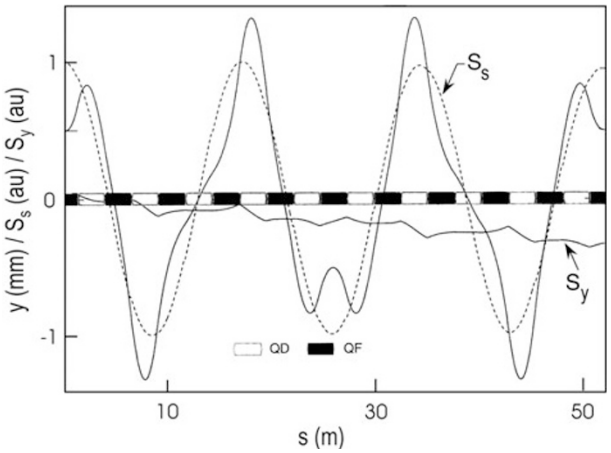

Fig. 10.1. Beam orbit (*solid line*) and spin transport in the SLC collider arc (Courtesy P. Emma, 1999)

10.8 Polarization Preservation in Storage Rings

For proton and deuteron accelerators, for which the polarization of the beam is produced at the particle source, the first requirement of maintaining a beam's polarization is preserving this polarization at injection into downstream accelerators. Ignoring synchro-betatron motion, this is easily achieved by orienting (using upstream spin rotators) the beam polarization so that it is aligned with the stable spin direction of the downstream transport line or storage ring.

A mismatch at injection results in a cosine-like reduction of the time-averaged beam polarization. Letting $(\cos\alpha_x, \cos\alpha_s, \cos\alpha_y)$ denote the orientation of the injected polarization $\mathbf{P}_{\rm inj}$ and $(\cos\beta_x, \cos\beta_s, \cos\beta_y)$ the orientation of the stable spin direction $\hat{\boldsymbol{n}}_{\mathbf{0}}$ in the laboratory reference frame, then the projection of the injected polarization vector $\mathbf{P}_{\rm inj}$ onto $\hat{\boldsymbol{n}}_{\mathbf{0}}$ is

$$\begin{aligned} \|\mathbf{P}\| &= \mathbf{P}_{\rm inj} \cdot \hat{\boldsymbol{n}}_{\mathbf{0}} \\ &= P_{\rm inj}(\cos\beta_x \cos\alpha_x + \cos\beta_s \cos\alpha_s + \cos\beta_y \cos\alpha_y) \ . \end{aligned} \tag{10.32}$$

The components of the time-average polarization one would measure at the injection point are then obtained by projecting the polarization onto the three coordinate axes:

$$P_y = \|\mathbf{P}\| \cos\beta_y, \quad P_x = \|\mathbf{P}\| \cos\beta_x, \quad P_s = \|\mathbf{P}\| \cos\beta_s \ . \tag{10.33}$$

A conceptual illustration is given in Fig. 10.2. At other locations in the ring, the measurable polarization components are obtained by performing a second projection using $\|\mathbf{P}\|\hat{\boldsymbol{n}}_{\mathbf{0}}(\boldsymbol{s})$ where $\hat{\boldsymbol{n}}_{\mathbf{0}}(\boldsymbol{s})$ is the stable spin direction at the point of interest.

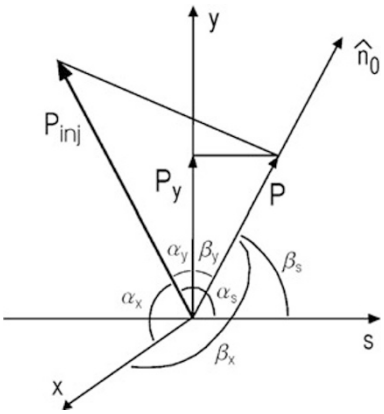

Fig. 10.2. Graphical representation showing the projection of the injected polarization P_{inj} onto the stable spin direction $\hat{n}_0$ at the injection point. The time-averaged vertical polarization one would measure at that point in denoted by P_y

Once the beam is successfully injected without loss of polarization, it must be ramped to high energy thereby encountering numerous depolarizing resonances along the energy ramp. With considerable effort, polarized proton beams were accelerated through many intrinsic and imperfection depolarizing resonances to GeV energies at the ZGS [16], Saturne [17], the AGS [18], and KEK [19]. The methods employed were based on overcoming each depolarizing resonance individually. In this section we review techniques used to overcome these resonances. In the next section we describe 'siberian snakes' which are used for preserving the beam polarization during the energy ramp. Proof of principle experiments with snakes were initially carried out at the Indiana University Cyclotron Facility (IUCF) [20]–[22]. Siberian snakes are now used in routine operation during acceleration of polarized protons at RHIC [23] and constitute the preferred method of polarization preservation for future high energy hadron accelerators.

10.8.1 Harmonic Correction

Harmonic correction of imperfection depolarizing resonances was used at the AGS [18] to ramp vertically polarized proton beams to about 22 GeV. There 96 correction dipoles were employed whose currents were programmed during the acceleration process such that the Fourier harmonics of the radially outward and longitudinal fields in the measured particle trajectories for the most nearby resonances were minimized. The Fourier harmonics are given by $a_n \cos n\theta + b_n \sin n\theta$, where n denotes the resonance harmonic of interest. As will be shown later, the resonance strength depends on the vertical beam displacement (in quadrupoles, for example, the nominally vertical polarization experiences a radial precession field with an off-axis beam). To eliminate depolarization, the coefficients a_n and b_n were experimentally adjusted to minimize the horizontal magnetic fields causing each imperfection resonance. Shown in Fig. 10.3 are traces on an oscilloscope from the AGS [18] showing

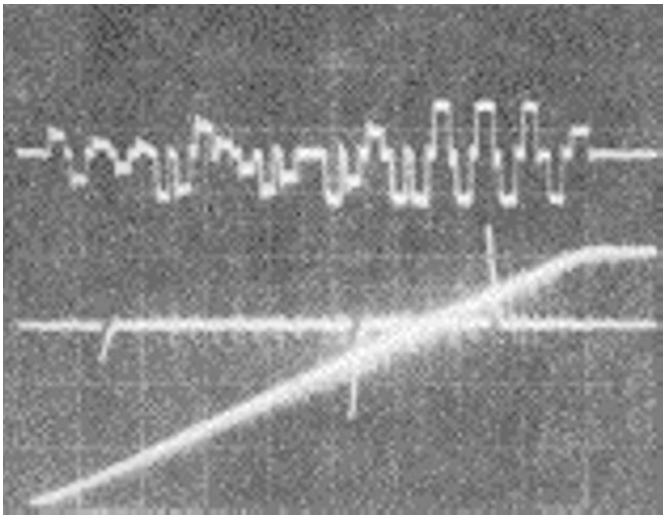

Fig. 10.3. Oscilloscope traces showing the currents in pulsed magnets during the energy ramp to 16.5 GeV/c at the AGS. Shown are the pulsed dipole currents (*top*), the pulsed quadrupoles currents (*middle*), and the main dipole current (*bottom*) (Courtesy A. Krisch, 1999)

the corrector dipole currents (top trace) and the main dipole current (bottom trace), which is proportional to the beam energy.

Harmonic correction methods [24]–[26] were also applied in the case of high energy electron beams at both HERA [27]–[29] and, deterministically, at LEP [30]. In electron accelerators, an initially unpolarized beam may after some time become polarized due to the emission of synchrotron radiation. This is known as the Sokolov–Ternov effect [31] which also predicts a maximum possible beam polarization of 92.4% for electrons. In practice however this level of polarization is not reached due to spin-orbit coupling caused by the trajectory oscillations which result from photon emission [3]. Minimizing the strength of the harmonics nearest the beam energy thus minimizes the

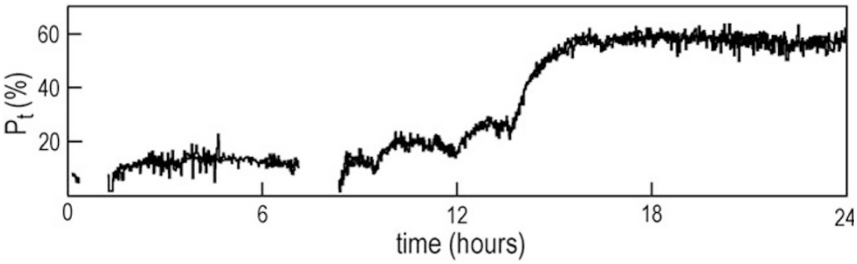

Fig. 10.4. Measured transverse beam polarization at HERA showing improvements gained using harmonic correction (Courtesy of the HERMES experiment, 2002)

influence of the depolarizing effects due to synchrotron radiation. At HERA and LEP, instead of empirically varying the whole closed orbit, closed orbit bumps were used to minimize the strength of the nearest imperfection resonances. A recent result from HERA is shown [29] in Fig. 10.4 obtained after implementing a new optic as intended for the HERA upgrade.

10.8.2 Adiabatic Spin Flip

The method of adiabatic spin flip, which was also used at the AGS, is based on the results of Froissart and Stora [32]. The Froissart–Stora formula, which describes the spin transport through a single, isolated imperfection or lowest-order intrinsic resonance, is

$$P_y(\infty) = \left(2e^{-\frac{\pi|\epsilon|^2}{2\alpha}} - 1\right) P_y(-\infty) \,, \tag{10.34}$$

where ϵ is the resonance strength (see Sect. 10.12 and [1]), $\alpha = \mathrm{d}\nu_0/\mathrm{d}\theta$, and $P_y(-\infty)$ or $P_y(\infty)$ refer to the initial and final polarizations, respectively.

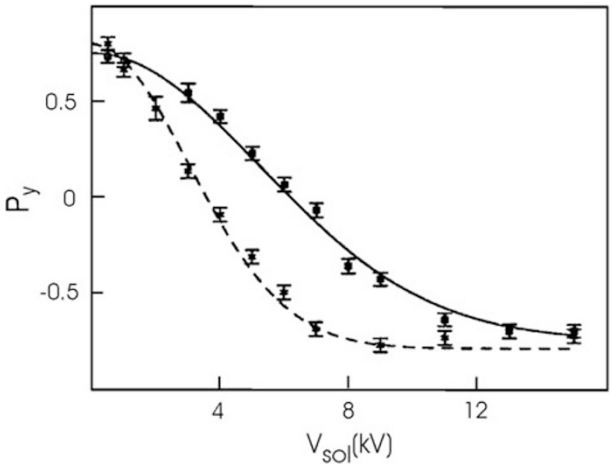

Fig. 10.5. Spin flip of a vertically polarized beam at the IUCF with kinetic energy 105.4 MeV and a frequency sweep range of 2 kHz. The estimated resonance strength at 15 kV applied voltage is $1.9{\times}10^{-4}$ (Courtesy A. Krisch, 1999)

The Froissart–Stora formula mandates that the spin of the orbiting particle will flip if the passage is slow and the resonance is strong (the argument in the exponent of (10.34) is large). This behavior has been verified by experiment [17, 33, 34]. An example taken from the IUCF cooler ring [34] is shown in Fig. 10.5. Here a solenoid was used to produce a sinusoidally varying longitudinal magnetic field of frequency f_{rf} and peak amplitude V_{sol}. This served to create a depolarizing resonance such that

$$\nu_0 \approx c_1 \pm \frac{f_{\rm rf}}{f_{\rm rev}} = c_2 \pm \left(\frac{f_{\rm rev} - f_{\rm rf}}{f_{\rm rev}} \right) , \tag{10.35}$$

where c_1 and c_2 are integers. In these measurements a frequency sweep of span 2 kHz centered about the revolution frequency was used. After each data point, the beam was dumped and a new beam was injected. The curves in Fig. 10.5 show the prediction by the Froissart–Stora equation computed for the measured resonance strength for two different ramp rates.

10.8.3 Tune Jump

Intrinsic depolarizing resonances were overcome at the AGS using the method of tune jump [18]. From the Froissart–Stora relation, if the resonance is crossed sufficiently quickly (the exponent approaches zero), then the polarization will be preserved. Therefore, as the spin tune $\nu_0 = G\gamma$ increases during acceleration, the resonance can be traversed without loss of polarization by rapidly shifting the vertical betatron tune, ν_y. A classic example [18] from the AGS was shown in Fig. 10.3 in which the current of the pulsed quadrupoles (middle trace) is depicted. To achieve this, strong pulsed quadrupoles and special ceramic beam pipes (to allow passage of the field) were required.

10.9 Siberian Snakes

The above mentioned correction schemes were anticipated to be of limited applicability when accelerating polarized beams to very high energies. The harmonic correction employed at the AGS was complicated and time consuming; the empirically found corrections also depended on the closed orbit of the accelerator, which was observed to drift with time and change between running periods. At very high energies, where the resonances will be overlapping due to an increase in the resonance strength with increasing energy (see (10.49) below), the method of adiabatic spin flip fails [35]. The method of tune jump is stopband limited since, for a very strong intrinsic resonance, the vertical betatron tune shift required to overcome the resonance may exceed the separation between the machine betatron resonances. Finally, the number of resonances to be crossed increases with energy. At the SSC, where there would have been more than 10^4 imperfection and first-order intrinsic resonances, overcoming each resonance individually clearly would have been impractical.

An ingenious arrangement of magnets was proposed [36, 37] by Derbenev and Kondratenko in 1976 (see also [13]). Use of this technique[4] would simultaneously overcome all imperfection and lowest-order intrinsic resonances by making the spin tune energy independent. A so-called type-1 snake rotates

[4] This scheme was dubbed 'siberian snake' by E. Courant.

the spin of each proton by 180 degrees about the longitudinal axis on each turn around the ring without changing the closed orbit outside of the snake. This forces the spin tune to be 1/2 and the stable spin direction $\hat{\boldsymbol{n}}_{\mathbf{0}}$ to lie in the horizontal plane. The resonance condition of (10.29) and (10.30) can therefore never be satisfied regardless of the beam energy: the condition for imperfection resonances with integer spin tune (10.29) is never satisfied and, for betatron tunes not equal to 1/2 (corresponding to half integer orbit resonances), intrinisic resonances (10.30) are also avoided. A type-2 siberian snake precesses the spin about the radial direction. A type-3 siberian snake precesses the spin about the vertical direction.

The most cost-effective construction of a siberian snake depends upon the energy range of interest. A siberian snake consisting of a solenoidal field (and skew quadrupoles for coupling correction) requires a field strength (given here for protons) of

$$\int B_{\parallel}\ \mathrm{d}l = \frac{mc\beta\gamma}{(1+G)e}\psi\,, \tag{10.36}$$

in which ψ ($= \pi$ for a full siberian snake) is the angle through which the spin is precessed. In this case, the required field integral depends linearly on γ. Due to technical constraints the field strength and magnet length cannot be increased indefinitely. Therefore siberian snakes made with solenoids are better suited for low energy operation.

Alternatively a 'conventional' siberian snake consisting of eight transverse field dipoles each of which precesses the spin by $\frac{\pi}{2}$ requires a field strength of

$$\int B_{\perp}\ \mathrm{d}l = \frac{mc\beta}{Ge}\psi \quad \text{(transverse snake)}\,, \tag{10.37}$$

which is independent of γ. This type of siberian snake therefore has the advantage that a single set of dipole operating currents suffices for all beam energies once the relativistic factor β is close to 1. However, in a dipole magnet, the orbit deflection angle is $\psi/G\gamma$ and so depends on the energy. For low beam energies ($\gamma < 10$), a siberian snake consisting of dipoles would thus require the construction of large and costly dipoles. Siberian snakes consisting of dipole magnets are therefore more suitable for operation at high beam energies.

With a single type-1 siberian snake, the one-turn spin transfer matrix evaluated at the orbital angle θ is

$$M = e^{-\mathrm{i}\pi\nu_0(\hat{\boldsymbol{n}}_{\mathbf{0}}\cdot\boldsymbol{\sigma})} = \left[e^{-\mathrm{i}\frac{G\gamma}{2}(\pi-\theta)\sigma_{\mathbf{y}}}e^{-\mathrm{i}\frac{\eta}{2}\sigma_{\mathbf{s}}}\right]\left[e^{-\mathrm{i}\frac{G\gamma}{2}(\pi+\theta)\sigma_{\mathbf{y}}}\right]\,, \tag{10.38}$$

where η gives the spin precession about the longitudinal in radians. Taking the trace of (10.38), the particle spin tune is

$$\cos\pi\nu_0 = \cos\left(\pi G\gamma\right)\cos\left(\frac{\eta}{2}\right)\,. \tag{10.39}$$

If the siberian snake is off ($\eta = 0$), then $\nu_0 = G\gamma$ as expected. With the snake fully turned on ($\eta = \pi$), then $\cos \pi\nu_0 = 0$ and $\nu_0 = 1/2$ (modulo 2π).

For a siberian snake design optimum for high beam energies, the use of transverse magnetic fields for spin precession has the unfortunate consequence of also deflecting the particle orbit. The design of a siberian snake therefore uses closed horizontal and vertical bumps so that the orbit outside of the snake region is unchanged (optical transparency). However this is achieved only at the expense of increased snake length which may become costly. Many different snake designs have been proposed. Some of the earlier designs by Steffen are given in [38]–[40] and the design currently used at RHIC is described in [41, 42] have been proposed. Shown in Fig. 10.6 is one such design consisting of alternating horizontal and vertical dipoles. This design is conveniently expressed as

$$\mathrm{V}\left(\frac{\pi}{2}\right)\mathrm{V}\left(-\frac{\pi}{2}\right)\mathrm{H}\left(\frac{\pi}{2}\right)\mathrm{V}\left(-\frac{\pi}{2}\right)\mathrm{H}\,(-\pi)\mathrm{V}\left(\frac{\pi}{2}\right)\mathrm{H}\left(\frac{\pi}{2}\right), \tag{10.40}$$

where H and V represent horizontal and vertical dipoles rotating the spin through the angle of the argument.

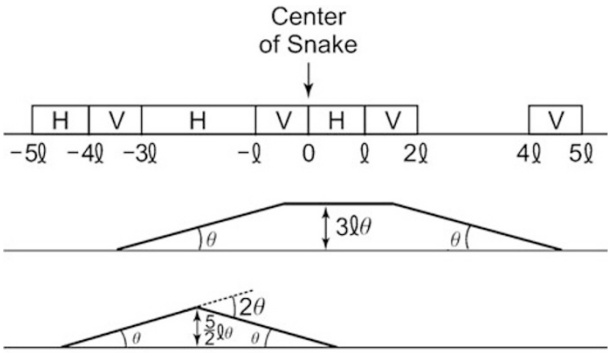

Fig. 10.6. A design of a type-1 siberian snake showing the geometry (*top*) and the design orbit in the vertical (*middle*) and horizontal (*bottom*) planes. The beam moves from the left to the right (Courtesy A. Chao, 1999)

In addition to preserving the polarization, it is often desirable to rotate the spin from vertical to longitudinal [4] at one of possibly many interaction points in a storage ring as is done at HERA [43], for example. An optically transparant spin rotator which does that was proposed by Montague [5, 44]. The spin rotation matrix R is given by

$$R = \mathrm{V}\,(\alpha)\,\mathrm{V}\,(-\alpha)\,\mathrm{V}\left(-\frac{\pi}{4}\right)\mathrm{H}\,(-\pi)\,\mathrm{V}\left(\frac{\pi}{4}\right)X\mathrm{V}\left(-\frac{\pi}{4}\right)\mathrm{H}\,(\pi)\,\mathrm{V}\left(\frac{\pi}{4}\right), \tag{10.41}$$

where α is an arbitrary precession angle and 'X' indicates the location of the interaction point. For transverse magnetic fields, the orbital bending angles

are obtained by the precession angle divided by $G\gamma$. In contrast to spin transformations for which the transfer matrices of each magnet do not commute, the small orbital deflections do essentially commute and are seen to sum to zero.

Radiation in strong vertical bending magnets, used in spin rotators for example, in an electron storage ring can cause excitation of vertical betatron motion which may then lead to depolarization due to the radial component of quadrupole fields [5]. In addition, when rotators are used to precess the polarization into the longitudinal direction, the horizontal motion excited by radiation in the arcs can cause depolarization in the vertical fields of the quadrupoles in the interaction regions. These depolarization mechanisms may be avoided by invoking spin matching conditions to obtain spin transparency [4, 26, 45].

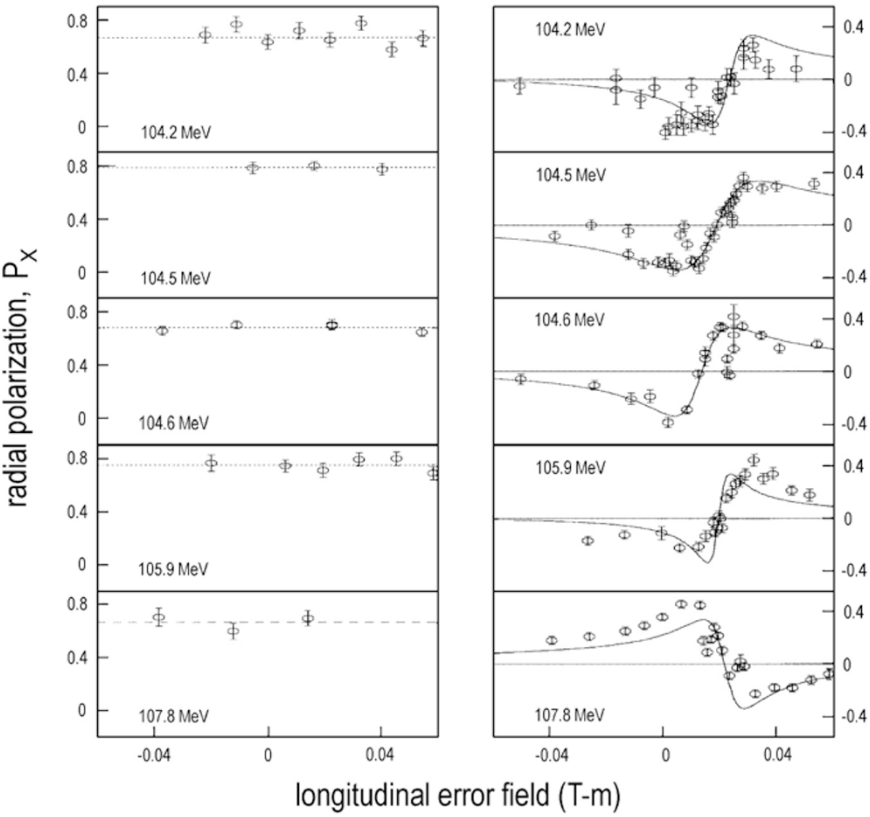

Fig. 10.7. Measurements of time-averaged radial polarization at the IUCF near a $G\gamma = 2$ imperfection resonance (at about 106.4 GeV) at 5 different beam kinetic energies with a 100% siberian snake on (*left*) and off (*right*)

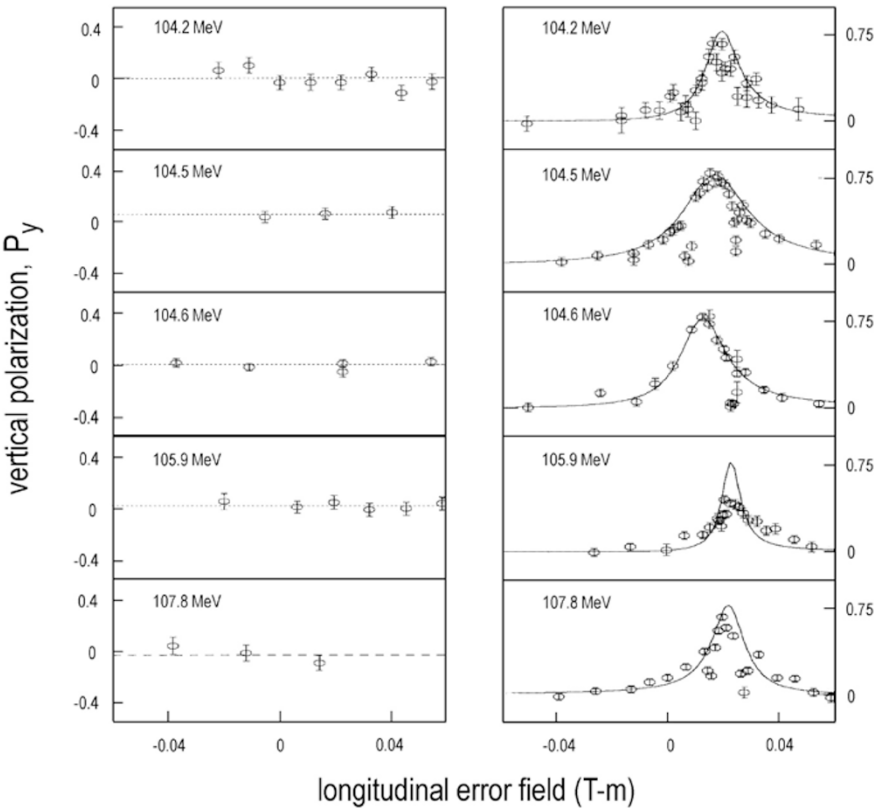

Fig. 10.8. Measurements of time-averaged vertical polarization at the IUCF near a $G\gamma = 2$ imperfection resonance (at about 106.4 GeV) at 5 different beam kinetic energies with a 100% siberian snake on (*left*) and off (*right*)

Interestingly, it was not until 1989 that the siberian snake concept was tested experimentally [20, 21]. Shown in Figs. 10.7 and 10.8 are measurements which demonstrated the use of siberian snakes for control of the beam polarization. Plotted are the time-averaged vertical and radial polarization measured at different beam kinetic energies in the vicinity[5] of the $G\gamma = 2$ imperfection resonance. The horizontal axis shows the strength of an error field introduced diametrically opposite to the siberian snake. In these measurements, the error field was set, the beam was injected, the polarization was measured, and then the beam was dumped. The polarization of the injected beam was always oriented to match the stable spin direction at the injection point; i.e. in the horizontal plane with the snake turned on or vertically with

[5] From the figures, the resonance was found to lie between 105.9 MeV and 107.8 MeV rather than at kinetic energy $(2 - G)/mG = 108.4$ MeV one might expect using $G\gamma = 2$. This was later explained by the presence of an unintentional type-3 snake in the accelerator.

no snake. From Fig. 10.7, with the snake turned on, the radial polarization was not affected by the nearby resonance. From Fig. 10.8, with the snake turned off, the measured time-averaged vertical polarization was observed to be less near the resonance. The curves in Figs. 10.7 and 10.8 were obtained using the periodic solution to the equatio of spin motion taking into account the presence of the type-3 snake.

It is worth mentioning that the presence of a siberian snake in an accelerator may introduce a new kind of resonance dubbed a snake resonance [46]. The snake resonance condition is given by $u\nu_{\rm res} = \nu_0 + n$ in which ν_0 $(=\frac{1}{2})$ is the spin tune determined by the snake and u and n are integers. These are relevant when the fractional betatron tune Q is 1/integer, which is not a condition under which an accelerator is typically operated. Nonetheless, the presence of snake resonances has been both predicted and verified experimentally [47].

10.10 Partial Siberian Snakes

In 1989 Roser [48] proposed an elegant and intuitive variant of the siberian snake called a partial siberian snake. These are magnetic devices which enable the polarization to be maintained when accelerating through imperfection resonances. They rotate the spin by a small fraction of π around a horizontal axis and have the advantage of reduced cost and less required space. At low beam energies, a partial snake consisting of dipoles does not induce too large an orbit excursion, while a solenoidal partial snake requires significantly less magnetic field than a full snake. As mentioned above the disturbance to the polarization at imperfection resonances can be minimized by minimizing certain harmonics in the fields on the closed orbit. Partial snakes imply the opposite approach, namely the snake induces a large predetermined imperfection onto the spin motion which dominates all other imperfections. Then during normal acceleration with the large resonance strength, the Froissart–Stora formula guarantees a full spin flip without loss of polarization. The polarization will flip again after passage through the next imperfection resonance.

The expression for the dependence of the spin tune on energy and the precession per turn was given in (10.39) and is shown in Fig. 10.9 for different percentages of applied longitudinal field ($\eta = \pi$ denotes a full snake which is designated in the figure by 100%). The diagonal line shows the spin tune with no snake. As can be seen, even a relatively weak ($\sim$ few %) snake can cause a significant deviation of the spin tune from $G\gamma$ during acceleration and a large spin tune gap thus avoiding the imperfection resonance at $\nu_0 = n =$ integer.

An example showing the first demonstration of the ability of partial siberian snakes to avoid imperfection depolarizing resonances, in this case at fixed beam energy, is shown in Fig. 10.10. With a 10% snake full polarization was maintained despite the applied error field. At the AGS a 5%

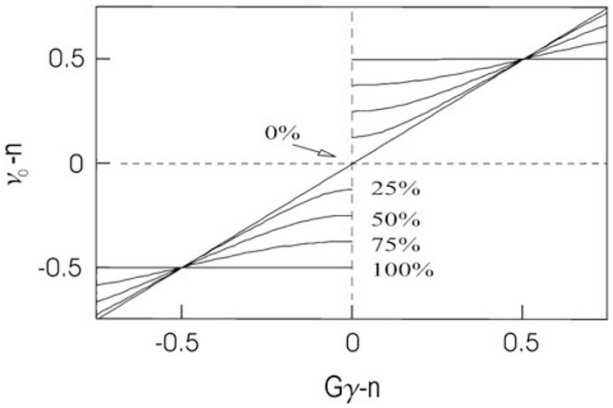

Fig. 10.9. The dependence of the spin tune on $G\gamma$ for various snake strengths (indicated by percentage of full 180 degree spin precession)

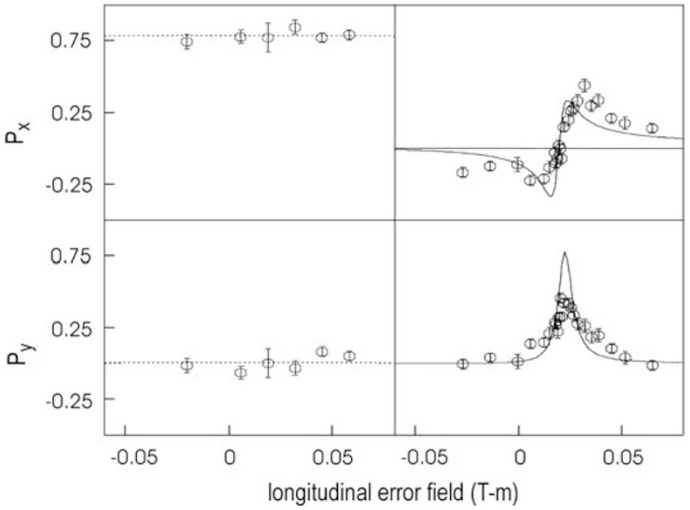

Fig. 10.10. Demonstration from the IUCF of polarization preservation in the vicinity of an imperfection resonance using a 10% partial siberian snake (*left*) and loss of polarization without the partial snake (*right*). In these measurements the kinetic energy of the beam was fixed at 105.9 MeV

partial siberian snake has been installed and is used routinely to ramp polarized protrons through numerous imperfection resonances to the required transfer energy ($\sim$ 25 GeV) for injection into RHIC [49, 50]. Note that for fixed beam energy, once the betatron tunes are known, the strength of the partial siberian snake could be set such that a nearby intrinsic resonance is also avoided.

10.11 RF Dipole

At the AGS, the many intrinisic resonances not avoidable the energy ramp are now overcome using an rf dipole magnet [51] (see also Sect. 3.10). From the Froissart–Stora equation (10.34), full spin flip may be expected if the resonance strength is large. The resonance strength may be artificially increased (see (10.48) below) by exciting a coherent vertical betatron oscillation thus inducing a complete spin flip [52]. If the location of externally induced resonance is placed close to an intrinsic resonance, then depending on the relative tune separation, phase, and strength, the induced resonance can be made to dominate the spin motion and full spin flip can be achieved [51]. At the AGS, the rf dipole is adiabatically turned on and off to avoid the emittance growth that would be observed with a pure impulse excitation [51].

10.12 Single Resonance Model

Until now we have avoided the use of complicated formulas and have presented basic concepts useful for practical applications of spin transport and preservation. In this section we define the resonance strength parameter ϵ used previously and show explicitly, for the case of an isolated resonance in the absence of siberian snakes, its effect on the beam polarization.

We rely on the work of Courant and Ruth [1], who expressed the magnetic fields in the Thomas-BMT equation in terms of the particle coordinates. They found that the equation of spin motion reduces to

$$\frac{\mathrm{d}S_x}{\mathrm{d}\theta} = -\kappa S_s - rS_y; \quad \frac{\mathrm{d}S_s}{\mathrm{d}\theta} = +\kappa S_x - tS_y; \quad \frac{\mathrm{d}S_y}{\mathrm{d}\theta} = +rS_x + tS_s \ , \quad (10.42)$$

where κ, r, and t are functions of the transverse coordinates of the particle orbit. In the cartesian coordinate system (with $\hat{x}$ radially outward, $\hat{s}$ along the beam direction, and $\hat{y}$ vertical) and ρ the local radius of curvature of the reference orbit, these variables are given by [1]

$$\begin{aligned} \kappa &= G\gamma - (1+G\gamma)\rho x'' \approx G\gamma \\ r &= (1+G\gamma)y' - \rho(1+G)\left(\frac{y}{\rho}\right)' \\ t &= (1+G\gamma)\rho y'' \ , \end{aligned} \quad (10.43)$$

where the derivatives are with respect to the longitudinal coordinate s.

Equation (10.42) can then be transformed [1] into an equivalent spinor representation, for which

$$\frac{\mathrm{d}\Psi}{\mathrm{d}\theta} = \frac{\mathrm{i}}{2} H\Psi \ . \quad (10.44)$$

Here H is the spinor precession matrix given by

$$H = \begin{pmatrix} -\kappa & -t - \mathrm{i}r \\ -t + \mathrm{i}r & \kappa \end{pmatrix} , \tag{10.45}$$

and Ψ is a two component complex spinor. In first approximation the function H is uniquely determined by the properties of the synchrotron. In the preceding analyses we have assumed that the function H is piecewise constant. As before the spin components are obtained by taking the expectation value of the Pauli matrix vector, $\boldsymbol{\sigma}$, i.e.,

$$S_i = \Psi^\dagger \sigma_i \Psi . \tag{10.46}$$

Due to the periodic nature of a synchrotron, the coupling term of (10.45) may be expanded in terms of the Fourier components, i.e.,

$$t + \mathrm{i}r = \sum_k \epsilon_k e^{-\mathrm{i}\nu^{\pm}{}_{\mathrm{res},k}\theta} , \tag{10.47}$$

in which θ is the particle's orbital angle, $\nu^{\pm}{}_{\mathrm{res},k} = k$ for imperfection resonances, $\nu^{\pm}{}_{\mathrm{res},k} = k \pm Q_y$ for the first order intrinsic resonances, and ϵ_k is the resonance strength which is given by the Fourier amplitude

$$\epsilon_k = \frac{1}{2\pi} \int (t + \mathrm{i}r) e^{\mathrm{i}\nu^{\pm}{}_{\mathrm{res},k}\theta} \, \mathrm{d}\theta . \tag{10.48}$$

For the case of an imperfection resonance, the resonance strength is given approximately by summing over the radial error fields encountered by a particle on the closed orbit in one turn around the ring:

$$\epsilon_k \approx \frac{1 + G\gamma}{2\pi} \sum_l \Delta s_l \, \frac{\partial B_x / \partial y}{B\rho} y e^{\mathrm{i}\nu_{\mathrm{res},k}\theta} , \tag{10.49}$$

where y is the transverse amplitude with respect to the magnet center, and Δs_l is the length of the lth integration step around the ring.

As an illustration of the previous results, we now show that a transverse imperfection resonance can also shift the spin tune ν_0. In the single resonance approximation [46, 53], the spin equation in the laboratory frame is given by

$$\frac{\mathrm{d}\Psi}{\mathrm{d}\theta} = -\frac{\mathrm{i}}{2} \begin{pmatrix} G\gamma & -\zeta \\ -\zeta^* & -G\gamma \end{pmatrix} \Psi, \quad \text{with} \quad \zeta = \epsilon \cdot e^{-\mathrm{i}\nu_{\mathrm{res}}\theta} , \tag{10.50}$$

in which ϵ is the resonance strength, ν_{res} is the resonance tune, and θ is the particle orbital angle around the accelerator. The spin motion near the imperfection resonance can be visualized by transforming the spin equation to the resonance precession frame (i.e., the reference frame in which the polarization vector does not precess if the spin tune is exactly equal to the resonant tune). Thus, considering

$$\Psi_k = e^{\mathrm{i}\frac{\nu_{\mathrm{res}}\theta}{2}\sigma_y} \Psi , \tag{10.51}$$

we obtain an expression for the effect of the imperfections,

$$\frac{\mathrm{d}\Psi_k}{\mathrm{d}\theta} = -\frac{\mathrm{i}}{2}\begin{pmatrix} -\delta & \epsilon \\ \epsilon^* & \delta \end{pmatrix}\Psi_1 \ , \tag{10.52}$$

with $\delta \equiv (\nu_{\mathrm{res}} - G\gamma)$. This can also be written as

$$\frac{\mathrm{d}\Psi_k}{\mathrm{d}\theta} = \frac{\mathrm{i}}{2}(\delta\sigma_y + \epsilon_R\sigma_x - \epsilon_I\sigma_s)\Psi_k \ , \tag{10.53}$$

where σ_i are the Pauli matrices and $\epsilon = \epsilon_R + i\epsilon_I$ the complex resonance strength. Equation (10.53) can be integrated easily to yield

$$\Psi_k(\theta_f) = e^{\frac{\mathrm{i}}{2}(\delta\sigma_y + \epsilon_R\sigma_x - \epsilon_I\sigma_s)(\theta_f - \theta_i)}\Psi_k(\theta_i) \ . \tag{10.54}$$

Then transforming back to the laboratory frame, we obtain

$$\begin{aligned}\Psi(\theta_f) &= e^{-\mathrm{i}\frac{\nu_{\mathrm{res}}\theta_f}{2}\sigma_y}e^{\frac{\mathrm{i}}{2}(\delta\sigma_y + \epsilon_R\sigma_x - \epsilon_I\sigma_s)(\theta_f - \theta_i)}e^{\mathrm{i}\frac{\nu_{\mathrm{res}}\theta_i}{2}\sigma_y}\Psi(\theta_i) \\ &= T(\theta_f, \theta_i)\Psi(\theta_i) \ . \end{aligned} \tag{10.55}$$

By expanding the exponential, the spin transfer matrix $T(\theta_f, \theta_i)$ for a single resonance may be calculated [46, 53]:

$$T(\theta_f, \theta_i) = \begin{pmatrix} ae^{\mathrm{i}\left(c - \frac{\nu_{\mathrm{res}}(\theta_f - \theta_i)}{2}\right)} & \mathrm{i}be^{-\mathrm{i}\left(d + \frac{\nu_{\mathrm{res}}(\theta_f + \theta_i)}{2}\right)} \\ \mathrm{i}be^{\mathrm{i}\left(d + \frac{\nu_{\mathrm{res}}(\theta_f + \theta_i)}{2}\right)} & ae^{-\mathrm{i}\left(c - \frac{\nu_{\mathrm{res}}(\theta_f - \theta_i)}{2}\right)} \end{pmatrix} \ , \tag{10.56}$$

with

$$\begin{aligned} b &= \frac{|\epsilon|}{\lambda}\sin\frac{\lambda(\theta_f - \theta_i)}{2}, \quad a = \sqrt{1 - b^2}, \\ c &= \arctan\left[\frac{\delta}{\lambda}\tan\frac{\lambda(\theta_f - \theta_i)}{2}\right], \quad d = \arg(\epsilon^*), \\ \delta &= \nu_{\mathrm{res}} - G\gamma, \quad \lambda = \sqrt{\delta^2 + |\epsilon|^2} \ . \end{aligned} \tag{10.57}$$

The spin tune on the closed orbit can be obtained from the trace of the one turn transfer map, $T(\theta + 2\pi, \theta)$ of (10.56), i.e.,

$$\cos\pi\nu_0 = a\cos(c - \nu_0\pi) \ . \tag{10.58}$$

Figure 10.11 shows the spin tune shift, $\delta\nu = G\gamma - \nu_0$, as a function of $G\gamma - 2$ for the special cases where $|\epsilon| = \sqrt{\epsilon_R^2 + \epsilon_I^2} = 0.0008$ and $|\epsilon| = 0.0015$. In both cases, for $G\gamma$ far away from the resonance tune, ν_{res}, one has $\delta \gg |\epsilon|$ and $a \approx 1$, so that $\nu_0 \approx G\gamma$. As $G\gamma$ approaches the resonance tune, the spin tune is shifted from $G\gamma$ by $\Delta\nu_0 = -|\epsilon|$ below the resonance and by $\Delta\nu_0 = |\epsilon|$ above the resonance, i.e., the spin tune is always shifted away from the resonance tune. Therefore at a given energy, the observed width of the vertical

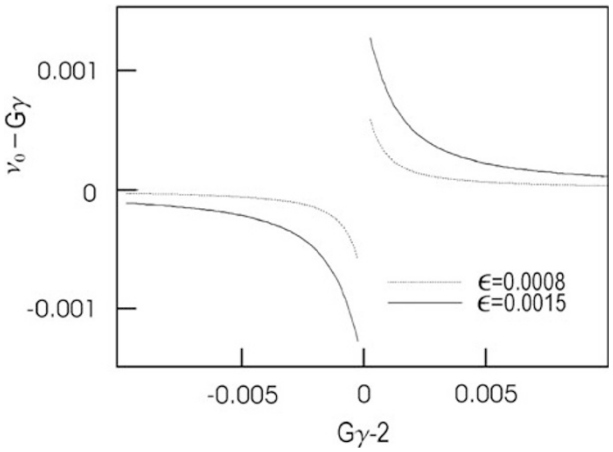

Fig. 10.11. Spin tune shift ($\nu_0 - G\gamma$) versus ($G\gamma - 2$) near an imperfection resonance, according to (10.58). The *dashed curve* corresponds to a resonance strength of magnitude 0.0008. The *solid curve* results for a resonance strength of 0.0015

polarization (in Fig. 10.8, for example) would always be increased when the effect of the imperfection resonance is included. The observed slope of the radial polarization at the fully compensated field value would also be lessened in magnitude. Figure 10.11 indicates that the effect of the imperfection resonance becomes important only in very close proximity to the resonance.

The solution of (10.52), decomposed into two eigenmodes, is

$$\Psi_{\pm} = e^{\pm \mathrm{i}\frac{\lambda\theta}{2}} \begin{pmatrix} \frac{\epsilon}{|\epsilon|}\sqrt{\frac{\lambda\pm\delta}{2\lambda}} \\ \mp\sqrt{\frac{\lambda\mp\delta}{2\lambda}} \end{pmatrix} , \tag{10.59}$$

where $\lambda = \sqrt{\delta^2 + |\epsilon|^2}$. The particle spin is given by a linear combination of the eigensolutions,

$$\Psi_1(\theta) = C_+\Psi_+ + C_-\Psi_- , \tag{10.60}$$

normalized such that $|C_+|^2 + |C_-|^2 = 1$. The component along the y axis is

$$\begin{aligned} S_y &= \Psi^{\dagger}\sigma_y\Psi \\ &= {\Psi_1}^{\dagger}\sigma_y\Psi_1 \\ &= \frac{\delta}{\lambda}\left(|C_+|^2 - |C_-|^2\right) + \frac{2|\epsilon|}{\lambda}\mathrm{Re}[C_+{C_-}^* e^{i\lambda\theta}] . \end{aligned} \tag{10.61}$$

For an initially vertically polarized particle, the time-averaged vertical polarization is found to be

$$\langle S_y\rangle = \frac{\delta}{\lambda}(|C_+|^2 - |C_-|^2) = \frac{\delta^2}{\lambda^2} = \frac{\delta^2}{\delta^2 + |\epsilon|^2} , \tag{10.62}$$

which is less than the initial polarization by an amount that depends on the resonance strength ϵ.

Exercises

10.1 Electrostatic Lenses and Muon Storage Rings

The muon anomolous magnetic moment, a_μ, now recognized to be about 0.001166, can be measured very accurately using electrostatic lenses with a transverse electric field. In the rotating reference frame, the spin precession is given by

$$\boldsymbol{\Omega} = -\frac{e}{m\gamma}\left(a_\mu B_\perp \gamma + (1+a_\mu)B_\parallel + \left(a_\mu\gamma - \frac{\gamma}{\gamma^2-1}\right)\frac{\boldsymbol{E}\times\boldsymbol{v}}{c^2}\right) . \quad (10.63)$$

Show that even the transverse electric field $\boldsymbol{E}$ does not contribute to spin precession when the Lorentz factor is[6]

$$\gamma = \sqrt{1+\frac{1}{a_\mu}} . \quad (10.64)$$

10.2 Spinors

This exercise provides practice with spinor-matrix algebra.

a) Using (10.10) find the spinor wave function for the spin basis $\boldsymbol{S} = [\boldsymbol{S}_x, \boldsymbol{S}_s, \boldsymbol{S}_y]$ with $\boldsymbol{S}_x = [1\ 0\ 0]$, $\boldsymbol{S}_s = [0\ 1\ 0]$, and $\boldsymbol{S}_s = [0\ 0\ 1]$.

b) Show that the Pauli matrices are unitary (${\sigma_j\sigma^\dagger}_j = I$) and Hermitian (${\sigma^\dagger}_j = \sigma_j$) with $\boldsymbol{\sigma}^\dagger \cdot \boldsymbol{\sigma} = 3I$.

c) Verify the compact form of the commutation relations:

$$\sigma_j\sigma_k = \delta_{jk}I + i\Sigma_m\epsilon_{jkm}\sigma_m, \quad (10.65)$$

where

$$\begin{aligned}\delta_{jk} &= 1 \ \text{ if } \ j = k \\ &= 0 \ \text{ if } \ j \neq k\end{aligned} \quad (10.66)$$

and ϵ_{jkm} is the Levi-Civita tensor defined by

$$\begin{aligned}\epsilon_{jkm} &= 0 \text{ if any two indices are equal} \\ &= +1 \text{ for even permutation of indices} \\ &= -1 \text{ for odd permutation of indices} .\end{aligned} \quad (10.67)$$

10.3 Spin Precession in Solenoidal Fields

Consider a vertically polarized beam traversing ($\boldsymbol{\beta} = \beta\hat{s}$) a longitudinal solenoid of field $\boldsymbol{B} = B_z\hat{s}$ of length l in the absence of any electric fields.

[6] Adapted from lecture notes of A. Chao (1999)

a) Show that the spin precession ϕ after traversal of the solenoid is given by

$$\phi = -\frac{e}{\gamma mc^2}\frac{l}{\beta}(1+G)B_z \ . \tag{10.68}$$

b) Suppose this solenoid is in a circular accelerator. By equating the centrifugal and Lorentz forces on the particle show that the magnetic rigidity is

$$B\rho = \frac{\beta E}{ec} \ , \tag{10.69}$$

where B is the vertical magnetic dipole field, and reexpress (10.68) in terms of the rigidity.

c) For spin polarization in a storage ring we have seen that spin precession by π per turn helps cancel various spin resonances. For the case of a proton beam with 100 MeV kinetic energy specify the required integrated field strength to achieve this.

10.4 Periodic Spin Motion

Using the expansion of the exponential

$$e^{\mathrm{i}\alpha\sigma_j} = \cos\alpha + i\sigma_j \sin\alpha \quad \text{where } j = x, s, y \ , \tag{10.70}$$

verify (10.25).

10.5 SLC '3-state experiment'

Assuming no resonant depolarization (that is pure spin precession) in the SLC arcs, show that the magnitude of the polarization at the interaction point (IP) can be obtained from three successive measurements of the longitudinal polarization at the IP by proper orientation of the incoming polarization with each measurement.

10.6 Type-3 Snakes

Let L represent a precession about the longitudinal axis.

a) Show that the configuration

$$\left[\mathrm{V}\left(-\frac{\phi}{2}\right)\mathrm{L}\left(+\frac{\chi}{4}\right)\mathrm{V}\left(+\frac{\phi}{2}\right)\right]\ \mathrm{L}\left(-\frac{\chi}{2}\right)\ \left[\mathrm{V}\left(-\frac{\phi}{2}\right)\mathrm{L}\left(+\frac{\chi}{4}\right)\mathrm{V}\left(+\frac{\phi}{2}\right)\right] \tag{10.71}$$

is does not introduce a net deflection, but produces a net spin precession about the vertical axis.

b) Draw the spin orientation and the particle orbit for the given magnet configuration.